ACS OMEGA

Open Access

http://pubs.acs.org/journal/acsodf

Article

Efficient Adsorption of Methylene Blue Using a Hierarchically Structured Metal−Organic Framework Derived from Layered Double Hydroxide

Ghulam Murtaza, Syed Shoaib Ahmad Shah, Asad Mumtaz, Ghayoor Abbas Chotana, Ayman Nafady, Md A. Wahab, and Manzar Sohail*

Cite This: *ACS Omega* 2024, 9, 16334−16345

Read Online

ACCESS | Metrics & More | Article Recommendations | Supporting Information

ABSTRACT: The growing concerns about environmental pollution, particularly water pollution, are causing an increasing alarm in modern society. One promising approach to address this issue involves engineering existing materials to enhance their effectiveness. A one-step solvothermal reconstruction approach was used to build an eco-friendly two-dimensional (2D) AlNiZn-LDH/BDC MOF composite. The characterizations confirm the formation of a metal−organic framework (MOF) at the layered double hydroxide (LDH) surface. The resulting synthesized material, 2D AlNiZn-LDH/BDC MOF, demonstrated remarkable efficacy in decontaminating methylene blue (MB), a model cationic dye found in water systems. The removal performance of 2D AlNiZn-LDH/BDC MOF was significantly higher than that of pristine 2D AlNiZn-LDH. This improvement shows the potential to increase the adsorption capabilities of nanoporous LDH materials by incorporating organic ligands and integrating meso-/microporosity through MOF formation on their surfaces. Furthermore, their kinetic, isothermal, and thermodynamic studies elucidated the adsorption behavior of this composite material. The results of synthesized MOF showed excellent removal efficiency (92.27%) of 10 ppm of MB aqueous solution as compared to pristine LDH. Additionally, the as-synthesized adsorbent could be regenerated for six successive cycles. This method holds promise for the synthesis of novel and highly effective materials to combat water pollution, laying the groundwork for potential advancements in diverse applications.

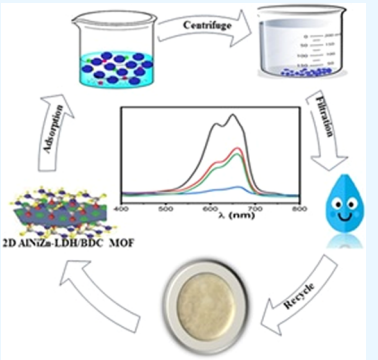

1. INTRODUCTION

Organic dyes are common pigments for coloring materials, such as plastic, rubber, paper, and textiles. However, their usage contributes significantly to dye pollution, a primary contaminant discharged into water bodies, such as rivers and lakes, by the printing and textile industries. The environmental impact of dye pollution is concerning due to the harmful nature of many organic dyes. They show potential threats to human health, and they are often teratogenic and carcinogenic. Moreover, these dyes are colorful and stubbornly adherent and present challenges in removal, exacerbating water pollution. Among the organic contaminants, methyl blue (MB) specifically received significant concern as MB finds widespread application in paints, textiles, magnetic toners, inks, highlighters, packaging materials, paper products, and asbestos content measurement. Consequently, its pervasive use intensifies its ecological footprint and amplifies the challenges of removing these dyes from aquatic systems. Human activities and the exponential growth of the economy and industries have propelled water pollution to emerge as a critical global concern.[1] The increasing demand for materials, driven by industrialization and overpopulation, has led to a profound redefinition of our way of life through various technologies.[2] Numerous methods have been reported to address this issue and to eliminate contaminants from wastewater. These include adsorption, extraction, biological degradation, membrane separation, coagulation, electrolysis,[3] precipitation, chemical reduction, and photocatalytic degradation.[4] Among these methods, adsorption provides a simple working principle, an efficient and cost-effective approach for dye removal.[5] Despite the advantages mentioned, this method avoids the generation of toxic byproducts.[6] Nevertheless, the efficiency of the adsorption process is largely dependent on selecting an appropriate adsorbent. Recent advancements have led to the development of several adsorbents, including graphene-based materials,[7] metal−organic frameworks (MOFs),[8] layered double hydroxides (LDHs),[9−11] and zeolites.[12] It is found that these materials hold significant promise in enhancing the efficiency of the adsorption process, offering new ways of tackling water pollution and advancing sustainable wastewater

Received: December 30, 2023
Revised: March 9, 2024
Accepted: March 12, 2024
Published: March 26, 2024

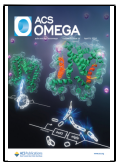

treatment practices. Moreover, the interaction between the adsorbent and adsorbate plays a critical role and mainly depends on the surficial functional groups, porosity, and surface area. Currently, it has been reported that thousands of MOFs are synthesized containing a variety of transition metal ions or clusters such as nickel.[13] In practical industrial applications, it is of great importance to select stable and environmentally friendly MOFs with high adsorption characteristics. Consequently, when selecting metal ions to synthesize MOFs, attention has gradually turned to light and nontoxic metal elements like Al. Aluminum metal is nontoxic, inexpensive, and more abundant than 8.3% of the Earth's crust by weight.[14] The transition metals have variable oxidation states, can make various complexes, and are used in heterogeneous catalyst synthesis such as Ni, Zn, etc.[15] The layered double hydroxides' (LDH) two-dimensional (2D) structure exposes metallic sites that effectively interact with the negative part of pollutants. However, this structure repels the positively charged parts, limiting its efficacy in adsorbing cationic materials.[16] However, advancements through surface modifications of LDHs have enhanced the attraction toward cationic pollutants. Various methods such as ion exchange, co-precipitation, and the reconstruction approach have been explored for LDH modification, enhancing the promising results.[17] Despite these advantages, improving the porosity and surface area remains a challenging task in optimizing LDHs for enhanced adsorption capabilities.

Inorganic−organic hybrid materials, commonly termed metal−organic frameworks (MOFs), exhibit distinctive structures characterized by their high surface area and porosity. The design of MOFs involves the intricate complexation of metal ions with organic ligands, enabling the creation of supramolecular structures with diverse functionalities.[18] These MOFs find applications across various fields, such as gas storage and molecular separation,[19] noise reduction,[20] energy storage,[21] catalysis,[22] drug delivery,[23] oxygen reduction reaction (ORR),[24,25] and adsorption.[26] Among the reported applications, in particular, MOFs have received significant attention for their potential in addressing water pollutant remediation.[27] In a study by Starukh et al., a composite of organo/Zn−Al LDHs was prepared using the reconstruction method[28] for MB adsorption in aqueous solution. The addition of dodecyl sulfate anions remarkably enhanced the affinity of organic/Zn−Al LDHs due to electrostatic attractions between the adsorbate and the surfactants. Similarly, Sharifi et al. prepared a CoZnAl-LDH/graphene oxide (GO) nanocomposite *via* ultrasonic mixing, addressing the challenge of adsorbing positively charged pollutants by LDHs.[29] Wang et al. demonstrated a synthetic compound, MgNiCo-LDH@ ZIF-67, as an adsorbent for Congo Red (CR) in water. This material exhibited excellent adsorption capabilities due to a substantial surface area and a hierarchical structure.[11] Nazir et al. developed CoAl-LDH @.ZIF-67 *via in situ* zeolite imidazolate framework (ZIF-67) growth on LDH, specifically targeting the removal of methyl orange (MO) and MB from water due to the porous nature of the composite.[25]

Despite the physical mixing of two materials like nanocomposites, incorporating the layered structure of LDHs with meso-/microporosity of MOFs within a single component holds the potential for significantly enhancing adsorption properties compared to their individual pristine structures. However, an intelligent synthetic strategy (ISS) involving the insertion of mesopores into layered structures represents an alternative approach to increase the adsorption capabilities of a hybrid hierarchical composite comprising LDHs and MOFs. Surprisingly, studies investigating cationic dye adsorption utilizing such a hybrid structure have remained relatively limited in recent reports. Generally, MOFs are composed of an assembly of metal ions and organic ligands, possessing superb potential scaffolds for catalytic materials.[30] In addition to the outstanding merits of MOFs, such as high specific surface area and chemical stability in water, they also serve as good supports to form well-dispersed catalysts, the long-term durability and thermal stability are improved due to the generated interface and generating a more accessible active site.[31] Therefore, the integration of MOFs with LDH offers a promising strategy to expand the scope of MOF applications by the suppression of the agglomeration of materials.[32]

In this context, we present a reliable and innovative ISS method designed to fabricate porous 2D AlNiZn-LDH/BDC MOF, integrating the *in situ* growth of MOF onto LDH. The resulting materials are anticipated to possess a surficial defective crystalline structure, exposing anionic groups (ligand COO^- species), aromatic ring, hydroxyl groups (OH^-), and embedded metal nodes. Furthermore, the material is expected to exhibit a defective surface and porosity compared to the pristine LDH structure. These characteristic features make the 2D AlNiZn-LDH/BDC MOF an attractive material for efficient cationic dye adsorption. Our investigation includes testing the cationic dye adsorption capability of 2D AlNiZn-LDH/BDC MOF, validating this concept.

2. EXPERIMENTAL SECTION

2.1. Materials. Aluminum nitrate nonahydrate, nickel nitrate hexahydrate, zinc nitrate hexahydrate, terephthalic acid (1,4-BDC), urea, sodium hydroxide, potassium hydroxide, ethyl alcohol, hydrochloric acid, N′N-dimethylformamide (DMF), methylene blue (MB) (molecular structural formula: $C_{16}H_{18}ClN_3S$; λ_{max}: 660 nm), and deionized (DI) water were employed in this study. All chemicals were used as purchased without distillation. Solutions were freshly prepared before the experiments.

2.2. Synthesis of Materials. *2.2.1. Trimetallic 2D AlNiZn-LDH Synthesis.* For the synthesis of trimetallic AlNiZn-LDH, a precise molar ratio of aluminum nitrate, nickel nitrate, zinc nitrate, and urea at 1:1:1:2 was mixed in 500 mL of DI water within a round-bottom flask equipped with a glass condenser. The solution was refluxed continuously at 95 °C for 2 days under continuous stirring. Subsequently, filtration was used to separate the synthesized light green precipitates, which were further subjected to multiple water washes to remove the unreacted species. Finally, the prepared AlNiZn-LDH was dried in a vacuum oven at 60 °C.

2.2.2. 2D AlNiZn-LDH/BDC MOF Synthesis. A novel porous AlNiZn-LDH-MOF was synthesized by a single-step solvothermal route employing a reconstruction method. The process involved the preparation of two separate solutions. Solution A was formulated by dispersing 1 mmol of AlNiZn-LDH in 30 mL of DMF, while solution B consisted of dissolving 2 mmol of terephthalic acid in 30 mL of DMF. Subsequently, solution A was mixed with solution B drop by drop in a separate beaker, and the resulting solution was sonicated for 1 h. Afterward, the solution was autoclaved at 130 °C for 24 h. Upon cooling, centrifugation at 8000 rpm was used to separate the synthesized material. The final brown material was washed frequently with DMF and ethyl alcohol to

https://doi.org/10.1021/acsomega.3c10524
ACS Omega 2024, 9, 16334−16345

remove residual components. Following the washes, the material was dried in a vacuum oven at 70 °C overnight. The schematic illustration in Figure 1 shows the synthesis of 2D AlNiZn-LDH/BDC MOF.

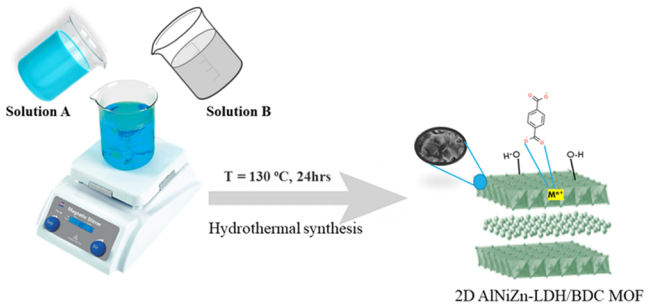

Figure 1. Schematic preparation of 2D AlNiZn-LDH/BDC MOF.

2.3. Characterization. All processed samples were subjected to powder X-ray diffraction (p-XRD) measurements using a Bourevestnik Dron-8 diffractometer outfitted with Cu K radiation (λ = 1.5406 Å) operated at 20 kV and 40 mA. A Nicolet iS10 FT-IR spectrometer was used to record the Fourier transform infrared (FT-IR) spectra of the KBr pellet within the 4000−400 cm^{-1} range. Visible spectra were recorded using a Hach Lange GmbH DR 3900 spectrophotometer. The thermal decomposition rate of the composite was analyzed by a thermogravimetric analysis instrument SDT650 TianmaV2 under an inert atmosphere. ζ-Potential measurements were conducted using a Wallius TM analyzer. Scanning electron microscopy (SEM) imaging, elemental mapping, and energy-dispersive X-ray spectroscopy (EDX) were determined with an FEI 450 Nova Nano-SEM electron microscope.

2.4. Dye Adsorption Experiment. In the adsorption experiment, the cationic dye methylene blue (MB) was used. Dye solutions containing various concentrations from 10 to 40 ppm were prepared. Then, 0.02 g of adsorbents (2D AlNiZn-LDH and 2D AlNiZn-LDH/BDC MOF) were dispersed in 0.025L of a 10 ppm dye solution under vigorous stirring. The solution was centrifuged at 4000 rpm for 5 min, following which a 10 mL aliquot of the remaining dye solution was extracted. The absorbance was measured by using a visible spectrophotometer. The efficiency and adsorption capacity of both 2D AlNiZn-LDH and 2D AlNiZn-LDH/BDC MOF were calculated by using the following equations.[33]

$$\text{adsorption efficiency (\%)} = \left[\frac{C_o - C_e}{C_o}\right] \times 100\% \quad (1)$$

equilibrium adsorption capacity

$$q_e = (C_o - C_e) \times \left[\frac{V}{m}\right] \quad (2)$$

adsorption capacity at time t

$$q_t = (C_o - C_t) \times \left[\frac{V}{m}\right] \quad (3)$$

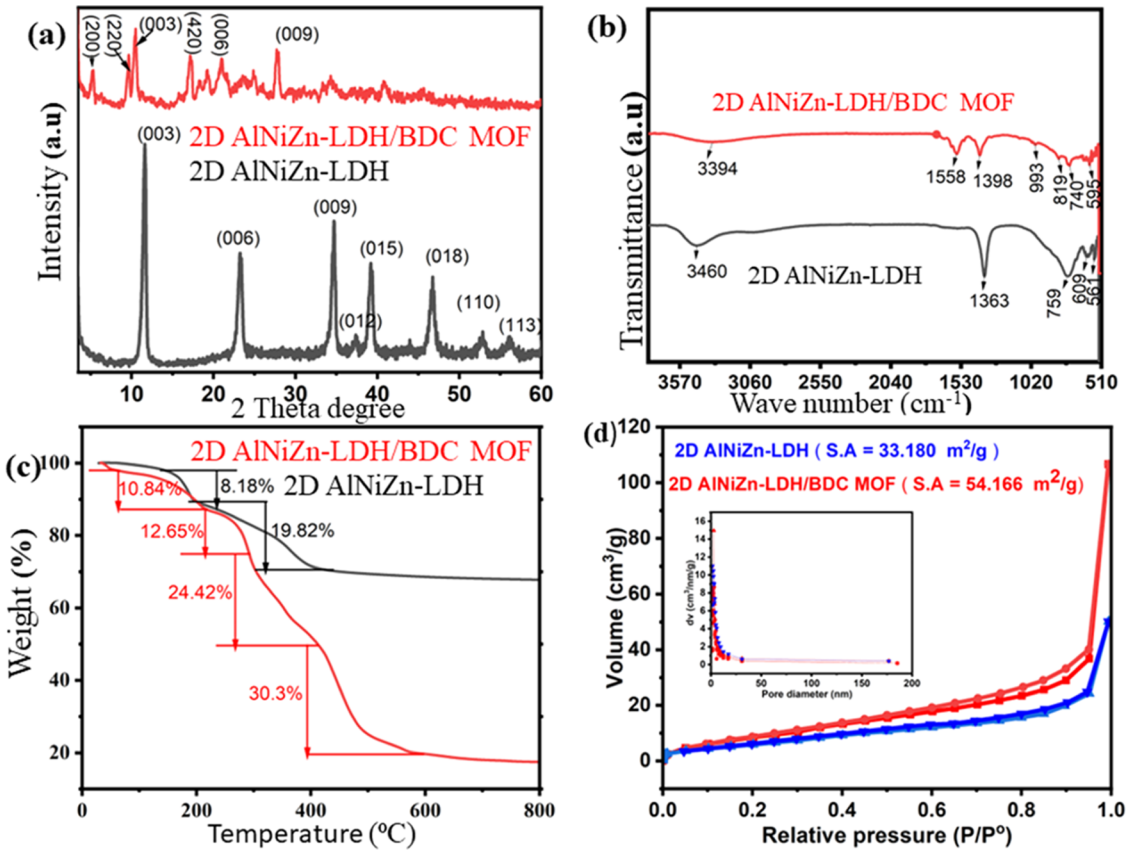

Figure 2. (a) XRD pattern of 2D AlNiZn-LDH and 2D AlNiZn-LDH/BDC MOF. (b) FT-IR spectra of 2D AlNiZn-LDH and 2D AlNiZn-LDH/BDC MOF. (c) TGA curve of 2D AlNiZn-LDH and 2D AlNiZn-LDH/BDC MOF. (d) BET adsorption isotherms of 2D AlNiZn-LDH and 2D AlNiZn-LDH/BDC MOF.

https://doi.org/10.1021/acsomega.3c10524
ACS Omega 2024, 9, 16334−16345

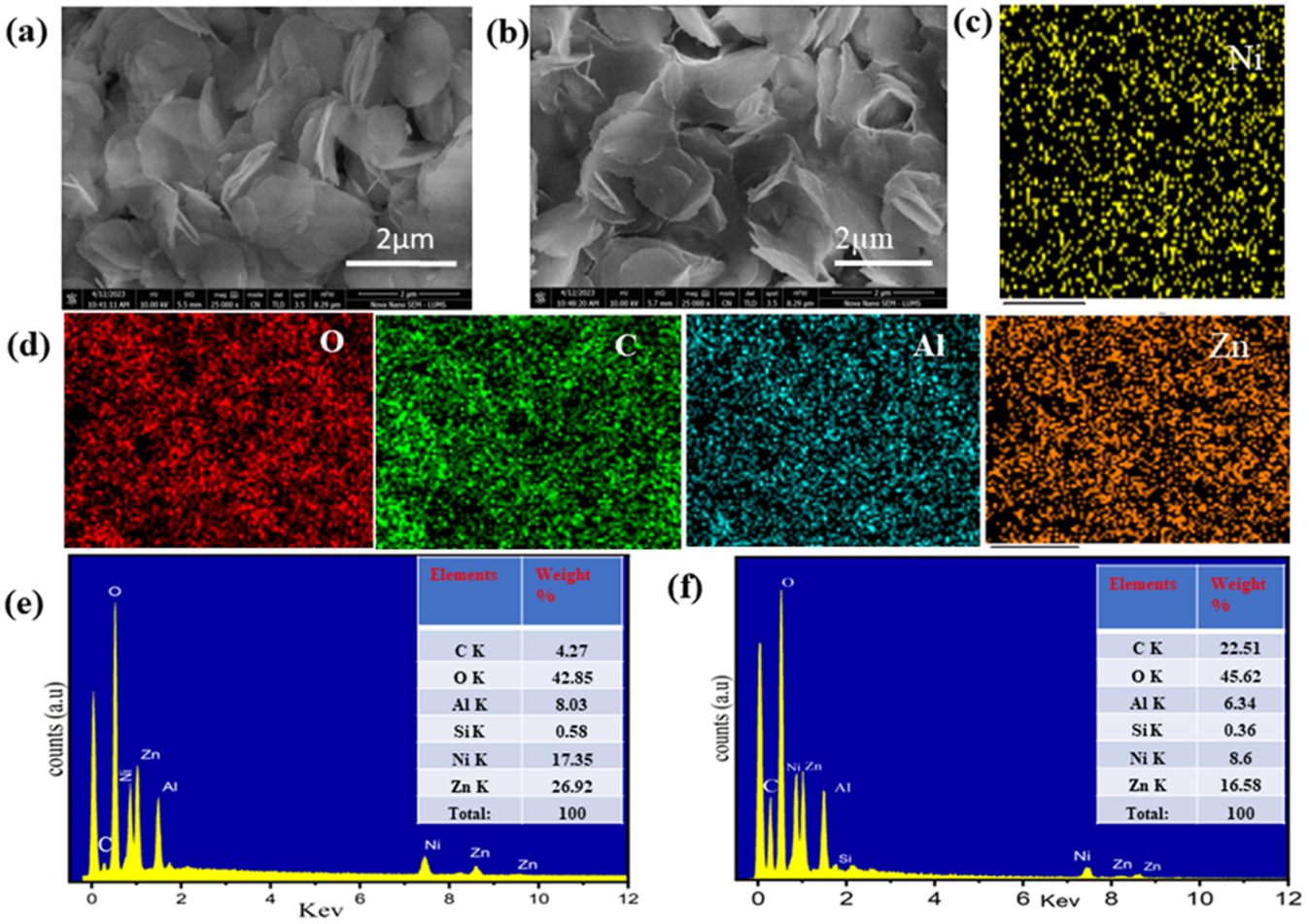

Figure 3. (a) SEM images of 2D AlNiZn-LDH. (b) SEM images of 2D AlNiZn-LDH/BDC MOF. (c,d) Elemental mapping of 2D AlNiZn-LDH/BDC MOF. (e) EDX spectrum of 2D AlNiZn-LDH. (f) EDX spectrum of 2D AlNiZn-LDH/BDC MOF.

where C_o is the starting concentration, C_e is the equilibrium concentration, C_t is the time-resolved dye concentration, V is the volume (L) of the dye solution, and m is the dry weight of the adsorbent (g).

The adsorption tests for MB using 2D AlNiZn-LDH and 2D AlNiZn-LDH/BDC MOF involved a systematic exploration of multiple parameters, such as dye initial concentration, temperature, adsorbent dose, pH, and contact time, while maintaining other variables constant to optimize the adsorption process. Upon completion of each experiment, the adsorbents were separated and collected by centrifugation once the experiments were finished. The adsorbents were dried and reused for the following experiment after being rinsed numerous times with a methanol-deionized water solution.

3. RESULTS AND DISCUSSION

3.1. Materials Characterization. The XRD diffraction pattern of pristine 2D AlNiZn-LDH, as shown in Figure 2a, revealed the distinct peaks at 2θ = 11.68, 23.1, 34.70, 39.27, and 46.77°, which is consistent with the characteristic atomic planes (003), (006), (009), (012), (015), and (018) associated with LDHs. This correspondence confirmed the formation of LDHs characterized by 2D hydrotalcite-like layered structures[34] (JCPDS 89−0460). According to Hine et al.,[35] XRD peaks occurring at 2θ < 30° represent the lamellar structure typical of hydrotalcite. The presence of the other two peaks labeled as (003) and (006) confirmed the successful preparation of 2D AlNiZn-LDH, indicating a well-defined and crystalline layered nature.[9] Particularly noteworthy is the prominence of the (003) plane at $2\theta \sim 11.6°$, representing the basal plane within the layered structure. The synthesis of 2D AlNiZn-LDH/BDC MOF involved the transformation of LDHs into MOFs through ISS. This process utilized a ligand to partially replace the surficial −OH groups in LDHs by linking with the exposed metallic ions.

The XRD pattern of the as-synthesized 2D AlNiZn-LDH/BDC MOF, as shown in Figure 2a, exhibited a difference compared to the XRD pattern of the pristine LDH. The characteristic peaks of the 2D AlNiZn-LDH/BDC MOF were observed at 2θ = 5.20, 9.60, 10.50, 17.20, 18.25, 19.25, 21.05, 23.65, 24.85, 26, 27.70, and 34.30°. Importantly, it was inferred that new peaks at 2θ = 5.20 and 9.60° appeared, while peaks at 2θ = 11.60, 23.40, and 34.70° were observed with slight shifts toward lower theta value and reduced intensity confirming the MOF formation over the LDH surface. However, the LDH layered structure was retained during the synthetic strategy of MOF. The peaks at 2θ = 5.20, 9.50, and 17.80° confirmed the formation of MOFs at the surface of pristine LDHs as reported in Al-BDC MOF, Ni-BDC MOF, and Zn-BDC MOF.[36]

The FT-IR spectrum of 2D AlNiZn-LDH (Figure 2b) exhibited a peak at 3460 cm^{-1}, representing the stretching vibration of the O−H groups of LDHs.[37] Additionally. another peak around 1363 cm^{-1} is associated with the symmetric stretching mode of the N−O bond of NO_3^- anions.[38] The

https://doi.org/10.1021/acsomega.3c10524
ACS Omega 2024, 9, 16334−16345

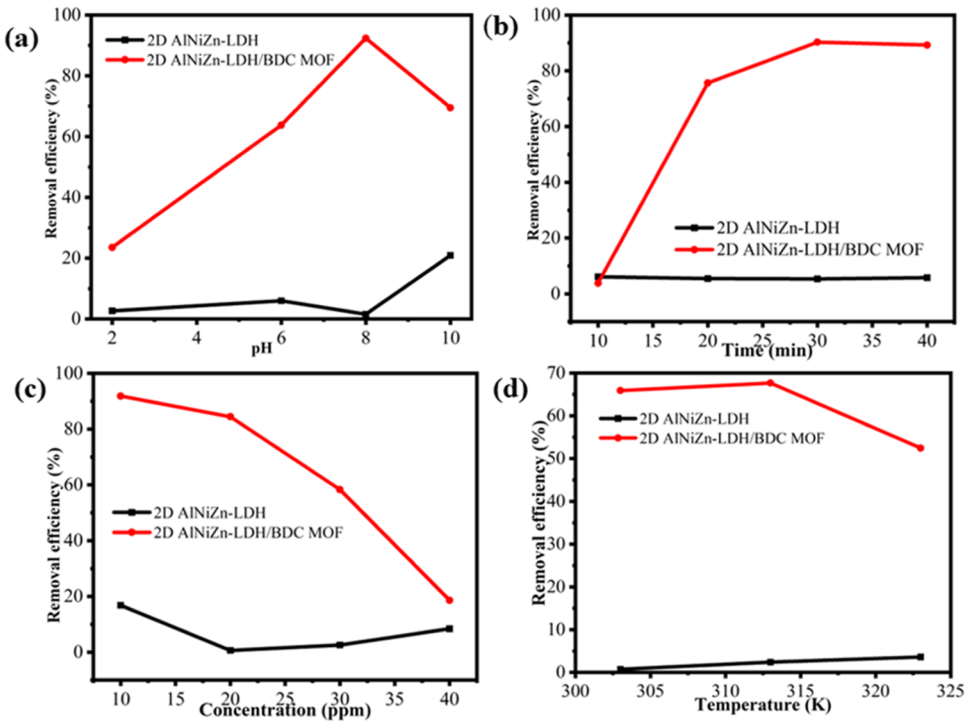

Figure 4. Illustration of the effect of (a) pH, (b) contact time, (c) concentration of dye, and (d) temperature on the adsorption. The contact time was 40 min. The stirring speed was 400 rpm. The temperature was 22 ± 3 °C. The pH maintained was neutral. The dosage of the adsorbent was 0.2 g and the concentration of dyes was 10 mg/L.

metal−oxygen stretching modes (M−O) within the lattice show absorption peaks in the 900−400 cm^{-1} range, where M represents Zn, Al, and Ni.[39] Furthermore, in the case of the FT-IR bands of 2D AlNiZn-LDH/BDC (Figure 2b), evidence successfully indicated the incorporation of terephthalate anions (COO^-) onto the surface of LDHs. A discernible band at 3394 cm^{-1} indicated the presence of hydrogen-bonded O−H groups from LDH in the composite. Vibrations corresponding to the (C−O) bond in COO^- and the (N−O) bond in NO_3^- are responsible for the peaks at 1558 and 1398 cm^{-1}, respectively.[40] Moreover, the characteristic benzene ring (phenyl mode) of the H_2BDC ligand possesses C═C bond bands at 1558 cm^{-1}.[41] Furthermore, M−O and O−M−O stretching vibrations in the range of 900−400 cm^{-1} also confirm the formation of MOFs.

The thermal stability assessment of synthesized 2D AlNiZn-LDH and 2D AlNiZn-LDH/MOF composites (Figure 2c) was conducted *via* thermogravimetric analysis (TGA) in an N_2 environment. The TGA revealed that two major weight losses occurred for each material. However, initially, a weight loss of 8.18% could be described as the removal of intercalated free or physisorbed water molecules. Subsequently, a second loss of 19.82% was observed from the dihydroxylation of hydroxide.[42] In contrast, the 2D AlNiZn-LDH/MOF showed four weight loss steps. The initial weight loss of 10.84% was ascribed to interlayer water loss, whereas the other weight loss of 12.65% (second) and 24.42% (third) is associated with the decomposition of the terephthalate ion, while the fourth weight loss of 30.3% could be associated with the hydroxylation of hydroxide layers. These distinct thermal degradation patterns observed in LDH and LDH/MOF composites confirm their structural formations and validate the intricate interaction between the constituent elements.[43]

The Brunauer−Emmett−Teller (BET) surface area analysis method was employed to measure specific surface area, pore diameter, and pore volume, as shown in Figure 2d. The results indicated that the surface area of the prepared 2D AlNiZn-LDH/BDC MOF was found to be 54.166 m^2/g, while the surface area of 2D AlNiZn-LDH was determined to be 33.180 m^2/g. The higher surface area observed in 2D AlNiZn-LDH/BDC MOF than that in 2D AlNiZn-LDH supports confirms the formation of MOF on the surface.[9]

The surface morphology study of trimetallic 2D AlNiZn-LDH in Figure 3a displays flake-like layered nanosheets, showing a resemblance to a sheet-like shape of ZnAl LDH.[43] These LDH nanosheets comprise interconnected nanoplate building blocks, forming an open-network structure. In contrast, the surface morphology of the as-synthesized 2D AlNiZn-LDH/BDC MOF (Figure 3b) differs slightly from that of 2D AlNiZn-LDH. The SEM of LDH/BDC MOF shows a leafy-like nanosheet. The elemental mapping of both LDH and LDH/BDC MOF (Figure 3c,d) confirmed the uniform distribution of elements like Ni, Zn, Al, C, and O within the synthesized materials. The EDX spectra of 2D AlNiZn-LDH (Figure 3e) and 2D AlNiZn-LDH/BDC MOF (Figure 3f) represented the weight percentages of aluminum, nickel, zinc, oxygen, and carbon. Additionally, the presence of BDC and the formation of the MOF on the surface of LDH were corroborated by an anticipated increase in the weight percentages of carbon (from 4.27 to 22.51%) and oxygen (from 42.85 to 45.62%). These findings further confirm the BDC's integration and the MOF's successful development on the LDH surface.

Another influencing factor affecting adsorbents' adsorption is their ζ-potential.[44] Therefore, the ζ-potential of 2D AlNiZn-LDH and 2D AlNiZn-LDH/BDC MOF was investigated across various pH levels. The results revealed significant

https://doi.org/10.1021/acsomega.3c10524
ACS Omega 2024, 9, 16334−16345

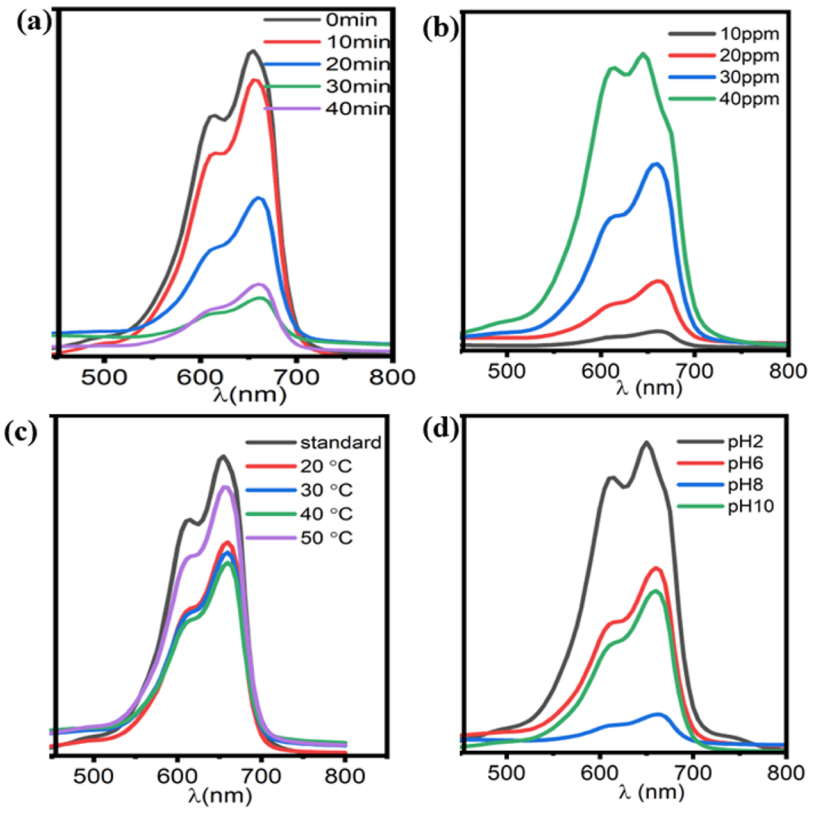

Figure 5. Visible spectra of adsorption of MB on the 2D AlNiZn-LDH/BDC MOF composite for different factors: (a) contact time, (b) concentration of dye, (c) temperature, and (d) pH. The contact time was 40 min. The stirring speed was 400 rpm. The temperature was 22 ± 3 °C. The pH maintained was neutral. The dosage of the adsorbent was 0.2 g and the concentration of the dyes was 10 mg/L.

differences: the LDH exhibited a positive surface potential of 4.64 mV in Figure S4a (Supporting Information), whereas the MOF displayed a negative surface potential of −26.29 mV in Figure S4b (Supporting Information) after coordination with the 1,4-BDC linkers. The difference in surface potentials suggests that the MOF holds a notably higher potential for effectively adsorbing cationic dyes than the pristine LDH. Such effectiveness can be attributed to the enhanced dye−adsorbent interactions from electrostatic attraction, complemented by hydrogen bonding and pi−pi interactions.

3.2. Adsorption Studies. *3.2.1. Effect of pH on Adsorption.* The effect of pH on the adsorption of MB was investigated using the as-synthesized 2D AlNiZn-LDH/BDC MOF. As shown in Figures 4a and 5d, different pH values ranging from 2 to 10 were used. The solution's pH was altered by adding a few drops of a 0.1 M aqueous solution of either hydrochloric acid or sodium hydroxide.[45] The finding suggested increased adsorption efficiency up to pH 8, followed by a subsequent decline in the efficiency at pH 10 (Figure 4a). A significant difference in adsorption capacity was evident between the 2D AlNiZn-LDH and 2D AlNiZn-LDH/BDC MOF composite at the optimal pH value (Figure S2). At the optimum pH, the 2D AlNiZn-LDH/BDC MOF composite displayed a considerably higher MB removal efficiency, reaching 92%, compared to that of pristine LDHs (Figure 4a). The ζ-potential value of 2D AlNiZn-LDH and 2D AlNiZn-LDH/BDC MOF at 8.6 pH are 4.64 and −26.29 mV, respectively, a negative charge on the surface of the synthesized MOF was found, which is favorable for the cationic dye to adsorb and shows maximum adsorption at particular pH (Figure S4). At lower pH, protonation of the carboxylic group of the MOF occurs, which weakly makes the cationic dye interact with the MOF. Under harsh conditions, such as strongly acidic or strongly basic media, the adsorption capacity was reduced due to the interference of ionic species from the surrounding environment. For example, at higher pH levels, the adsorption capacity of MB is reduced because of the presence of substantial OH^- in the basic solution, leading to a decrease in the adsorption capacity process.

3.2.2. Effect of Contact Time on Adsorption. The adsorption studies were influenced by the contact time, wherein intervals of 10, 20, 30, and 40 min were used to calculate the quantity of MB removed from the solution at each interval time. An analysis of visible spectra revealed a notable trend: increasing adsorption of the MB onto the 2D AlNiZn-LDH/BDC MOF composite (Figure 5a) compared to pristine LDH (Figure S1a) as time progressed. While the adsorption capacity of LDH remained constant, the MOF exhibited a gradual increase in adsorption toward MB up to 30 min, plateauing thereafter (Figure S2b). Specifically, the 2D AlNiZn-LDH/BDC MOF composite showed a remarkable 92% removal efficiency within 30 min (Figure 4b), in contrast to the 10% exhibited by pristine LDHs. Further prolonging the contact time showed no significant variance in adsorption. This observed phenomenon suggests that active sites within the synthesized materials were initially readily available for adsorption. However, as time elapsed, these active sites became saturated by adsorbents, preventing further adsorption.

3.2.3. Effect of Concentration of Dye on Adsorption. Different concentrations of dye, ranging from 10, 20, 30, and 40 ppm, were employed to determine the influence of concentration on both 2D AlNiZn-LDH and amides (Figure

https://doi.org/10.1021/acsomega.3c10524
ACS Omega 2024, 9, 16334−16345

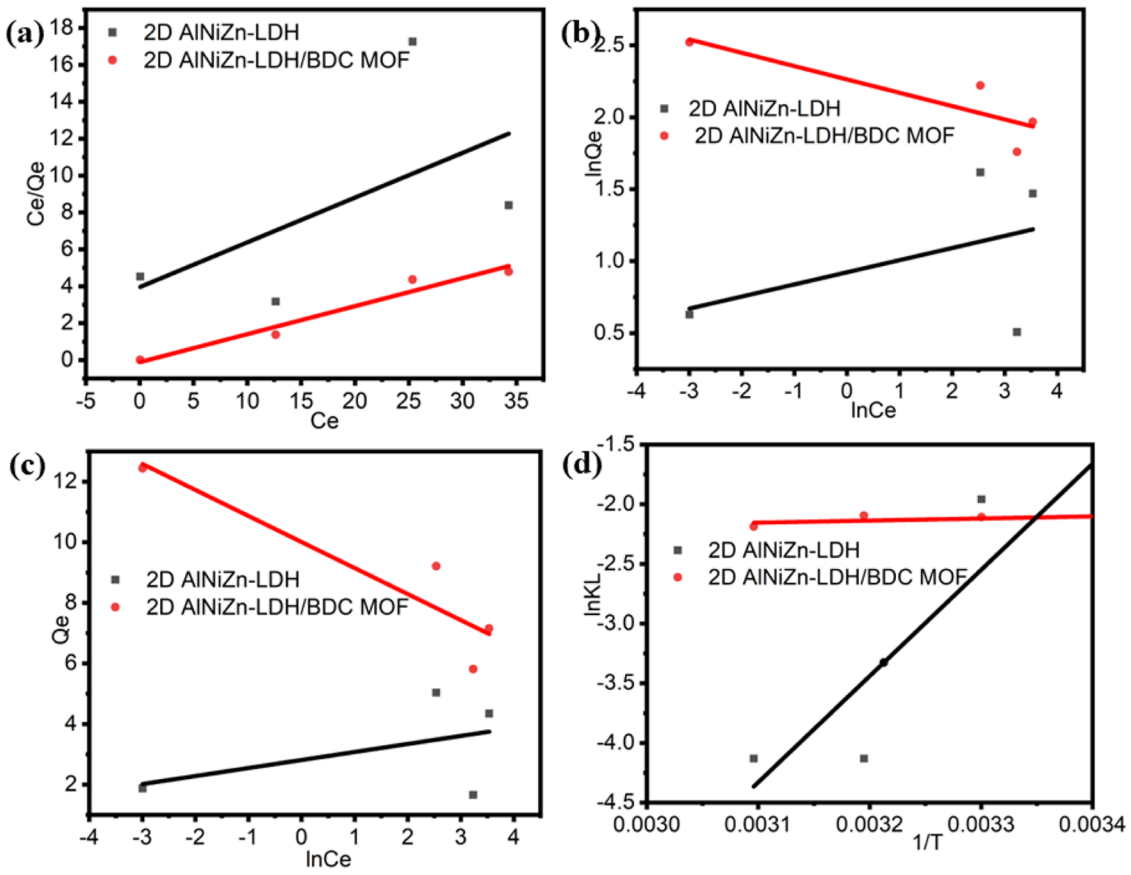

Figure 6. (a) Langmuir isothermal model. (b) Freundlich isothermal model. (c) Temkin isothermal model. (d) Thermodynamic model.

S1b) and the 2D AlNiZn-LDH/BDC MOF composite (Figure 5b), showing a relationship between concentration and adsorption efficacy. At lower dye concentrations, it is presumed that enough active sites are available for adsorption, resulting in higher removal effectiveness. However, it is shown that as the MB concentration increases, the MOF's efficacy in removing the dye diminishes. This reduction in effectiveness is attributed to the saturation of active sites on the material at higher concentrations, leaving dye molecules unadsorbable within the medium (Figure 4c). However, while the adsorption capacity of LDH toward MB remains relatively unchanged across varying dye concentrations, the MOF exhibits capacity dependency on the dye concentration (Figure S2c).

3.2.4. Effect of Temperature on Adsorption. A range of temperatures (293, 303, 313, and 323 K) was selected to investigate the adsorption behavior of MB concerning both the as-synthesized 2D AlNiZn-LDH and 2D AlNiZn-LDH/BDC MOF composite. The analysis revealed distinctive trends regarding the impact of temperature on the adsorption process. It has already been observed that the MOF composite showed higher removal efficiency than LDH (Figure 4d). In this study, the temperature exhibited no discernible effect on the adsorption of LDH (Figure S1c), whereas the MOF displayed varying adsorption behavior in response to temperature changes, as observed in Figures 5c and S2d. The MB adsorption capacity over the MOF composite showcased an ascending trend up to 313 K, beyond which a decline in adsorption occurred, initiating the process of desorption. This observed phenomenon might be attributed to the solventization effect on the absorbent and larger dye molecules with temperature changes. Moreover, as temperature increased, it likely increased the mobility of dye molecules, thereby diminishing the adsorption capacity of the composite, as supported by previous studies.[46]

3.2.5. Effect of Concentration of Adsorbent on Adsorption. Different amounts of the adsorbent, ranging from 5 to 40 mg per 25 mL, were employed in the adsorption experiment using a 10 ppm MB solution (as shown in Figure S3). The results indicated a direct correlation between the concentration of the adsorbent and the adsorption capability of MB onto the MOF. As the quantity of the adsorbent increased, there was a corresponding enhancement in the capacity of MB to adsorb onto the MOF. However, after careful evaluation, it was determined that 20 mg of the adsorbent, specifically the 2D AlNiZn-LDH/BDC MOF composite, represented the optimum quantity for subsequent adsorption experiments.

3.3. Equilibrium Adsorption Isotherm Study. Adsorption isotherm studies were performed at constant temperature conditions to determine the association between the amount of MB adsorbed and the MB concentration at equilibrium. Three adsorption isothermal models, namely, Langmuir,[47] Freundlich,[48] and Temkin,[49] were used to analyze the experimental data. Langmuir isotherm model operates under the assumption of homogeneous adsorption sites distributed across the adsorbent surface. According to this model, adsorption cannot progress beyond the monolayer when the adsorbate occupies a site. The Langmuir equation can be written as

$$\frac{C_e}{q_e} = \frac{1}{q_{maxKL}} + \frac{C_e}{q_{max}} \quad (4)$$

https://doi.org/10.1021/acsomega.3c10524
ACS Omega 2024, 9, 16334−16345

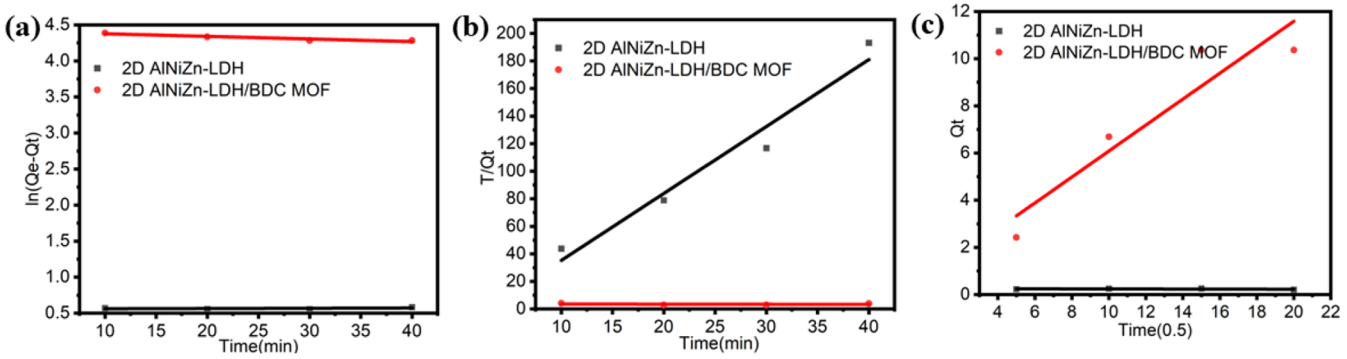

Figure 7. (a) Pseudo-first-order kinetic model. (b) Pseudo-second-order kinetic model. (c) Intraparticle diffusion kinetic model.

where KL ($L{\cdot}mg^{-1}$) stands for the affinity constant, which is connected to the adsorption binding energy, and the maximum adsorption capacity of the adsorbate is given by q_{max} ($mg{\cdot}g^{-1}$).

The Freundlich model is an empirical equation that also expresses isothermal parameters. This equation assumes that a multilayer adsorption process can cause adsorption on a heterogeneous surface. Freundlich equation can be written as

$$\ln q_e = \ln k_f + \left(\frac{1}{n}\right)\ln C_e \tag{5}$$

The Freundlich model adsorption constants for absorbent surface heterogeneity are K_f and n. n measures the adsorption-driving force ($0 \leq 1\ n \leq 1$).

The Temkin isotherm model's central tenet is that adsorbent−adsorbate interactions linearly reduce the heat of all of the adsorbate molecules in a layer. Moreover, the maximal binding energy of absorbent−adsorbate sites is spread uniformly.[50]

$$q_e = \frac{RT}{b}\ln A + \frac{RT}{b}\ln C_e \tag{6}$$

The equilibrium binding constant is A and the greatest binding energy is b (kJ = mol^{-1}). The absolute temperature (K) is given by T, while the universal gas constant (8.314 J mol^{-1} K^{-1}) is given by R.

An isothermal study was performed on MB adsorption using the as-synthesized materials, namely, 2D AlNiZn-LDH and 2D AlNiZn-LDH/BDC MOF, by fitting three models, such as Langmuir, Freundlich, and Temkin. Their graphical expressions are shown in Figure 6 and the results are also summarized in Table S1. The data analysis indicated that the Langmuir model exhibited a superior fit for MB adsorption, as evidenced by its greater R^2 value, suggesting monolayer adsorption. Correlation coefficient (R^2) values of synthesized materials 2D AlNiZn-LDH and 2D AlNiZn-LDH/BDC MOF for MB in the Langmuir model are (2D AlNiZn-LDH R^2 = 0.51) and (2D AlNiZn-LDH/BDC MOF R^2 = 0.95). These results affirm the efficiency of the *in situ* synthesized MOF as a highly effective adsorbent for removing MB from water. The relationship between C_e *versus* Q_e and T *versus* Q_t for LDH and MOF has been mentioned in Figure S5a,b.

3.4. Adsorption Kinetics Study. The adsorption capacity data has been analyzed by fitting it into the first-order, pseudo-second-order, and intraparticle diffusion models. According to the pseudo-first-order model, the adsorption rate is proportional to the total number of bared sites. Pseudo-first order represents very fast solid−liquid adsorption.[51] On the other hand, as per the pseudo-second-order model, the adsorption rate at the binding site is proportional to the square of the number of vacant sites.[52] The adsorption capacity and the intraparticle diffusion model agree due to the porosity of MOF. This model assumed that the diffusion of the adsorbate through the pores of the adsorbent material is the rate-limiting phase.[53] The equations representing the pseudo-first-order, pseudo-second-order, and intraparticle diffusion models are shown below.

$$\text{pseudo first order model: } \ln(q_e - q_t) = \ln q_e - k_1 t \tag{7}$$

$$\text{pseudo second order model: } \frac{t}{q_t} = \frac{1}{k_{2q2_e}} + \frac{t}{q_e} \tag{8}$$

$$\text{intra-particle diffusion model: } q_t = a + k_{int}t\frac{1}{2} \tag{9}$$

q_e, q_t, and t represent the equilibrium, time-resolved, and time, respectively. k_1 (min^{-1}) is the pseudo-first-order rate constant. k_2 (g mg^{-1} min^{-1}) is the pseudo-second-order rate constant. K_{int} is the boundary layer thickness constant, and a is the intraparticle diffusion rate.

The kinetic study was also conducted on the synthesized materials, revealing a remarkable correlation between the adsorption mechanism of MB dye and its binding pathway on both the 2D AlNiZn-LDH and 2D AlNiZn/BDC MOF composites (Figure 7). Table S2 presents the kinetic parameters obtained from fitting the data and the corresponding R^2 values for the prepared LDH and MOF. Among the various kinetic models explored, the adsorption capacity data of 2D AlNiZn-LDH/BDC MOF exhibits the most robust adherence to the pseudo-first-order model, boasting an R^2 value of 0.99. This substantiates the physisorption of MB dye onto the composite material.[54]

3.5. Adsorption Thermodynamics Study. The following equations explain the thermal behavior of MB adsorption onto 2D AlNiZn-LDH and 2D AlNiZn-LDH/BDC MOF adsorbents

$$\Delta G = -RT\ln K^\circ$$

$$\ln K^\circ = \frac{\Delta S^\circ}{R} - \frac{\Delta H^\circ}{RT}$$

K°, R, and T are equilibrium constant, universal gas constant, and temperature, respectively.

Thermodynamic parameters pertaining to both 2D AlNiZn-LDH and 2D AlNiZn-LDH/BDC MOF are presented in Table S3, and the thermodynamic graph is shown in Figure 6d. The positive ΔG° value observed for the as-synthesized MOF

https://doi.org/10.1021/acsomega.3c10524
ACS Omega 2024, 9, 16334−16345

revealed that the adsorption process is nonspontaneous, while negative ΔH° indicates an exothermic MB adsorption process. Similarly, the negative ΔS° value for the 2D AlNiZn-LDH/BDC MOF suggests a reduction in randomness during the adsorption process.[55]

3.6. Adsorption Mechanism of 2D AlNiZn-LDH/BDC for MB Dye. The adsorption of dye molecules from an aqueous solution is affected by its surface chemistry, textural features, and adsorbent−adsorbate interactions like stacking, electrostatic interaction, hydrogen bonding, acid−base interaction, ion exchange, and coordination. Assessing the surface chemistry of the as-synthesized2D AlNiZn-LDH/BDC MOF, MB dye was chosen to evaluate the adsorption performance of the prepared porous material. The adsorption spectra of MB solutions with varying concentrations were recorded at λ_{max} = 660 nm. Intermolecular forces primarily influence the interaction between the adsorbent surface and the adsorbate. The adsorbent surface, *i.e.*, the prepared MOF has a carboxylate functional group (COO^{-}), OH^{-}, and aromatic ring, while the adsorbate surface *i.e.*, the MB has a benzene ring, where the −N and $-S^{+}$ groups displayed an adsorption mechanism due to high electrostatic interaction, $\pi-\pi$ interaction, and H-bonding. The high MB adsorption capacity of the synthesized MOF for MB was due to three interactions illustrated in Figure 8.

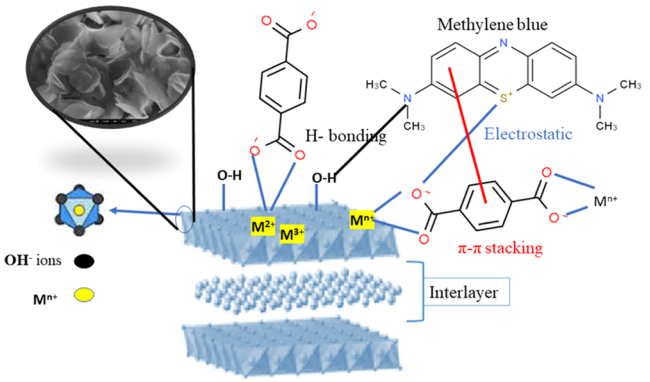

Figure 8. Possible interactions between the adsorbent and MB.

(i) The electrostatic interactions between the electron-rich oxygen and cationic dyes.

(ii) Hydrogen bonding between the OH group of the adsorbent 2D AlNiZn-LDH/BDC MOF and dimethylamino ($-N(CH_3)_2$) group of dyes.

(iii) $\pi-\pi$ stacking interaction between the phthalic acid unit in the structure of 2D AlNiZn-LDH/BDC MOF and the benzene ring in the dye molecule.[56]

3.7. Reusability of 2D AlNiZn-LDH/BDC MOF. Regeneration is an important factor in an ideal absorbent. Following rapid adsorption, a desorption experiment was conducted to assess the process. The 2D AlNiZn-LDH/BDC MOF adsorbent was washed with either 0.1 M HCl or NaOH, followed by agitating for 20 min in an alcoholic solution. Subsequently, the separated adsorbent was rinsed multiple times with ethanol and DI water. The dried adsorbent demonstrated reusability potential, being successfully reused for up to six cycles in the reusability experiment. The stability of the material is determined by comparing the XRD pattern of MOF before and after reusability, as shown in Figure 9a−c.

The synthesis involved a series of techniques to effectively convert LDH into MOF. These techniques were implemented as follows: (i) environmentally friendly synthesis of 2D trimetallic AlNiZn-LDH nanosheets, (ii) improvement in the interaction between LDH and organic linker BDC, and (iii) the solvothermal assisted growth of organic linker crystal on the surface of LDH nanosheets. As a result of these methodologies, the prepared LDH/MOF exhibited significantly improved adsorption rates, demonstrating a higher adsorption percentage in notably shorter durations compared to previously reported MOFs, as detailed in Table 1.

Table 1. Comparison Study of the Prepared 2D AlNiZn-LDH/BDC MOF with Different MOFs Reported Earlier for the Methylene Blue (MB) Adsorption Percentage

adsorbent/MOF	adsorbent amount(g/L)	time (min)	adsorption (%)	refs
CuBTC MOF	12.5	2880	22−33	52
MOF-545(Fe)	0.1	300	38.2	53
2D Cu(II)-MOF	1.2	60	92	57
3D CuBTC MOF	0.5	350	72.5	54
Zif-67@CoAl-LDH	0.05	100	79.9	58
2D AlNiZn-LDH/BDC MOF	0.02	40	92	this work

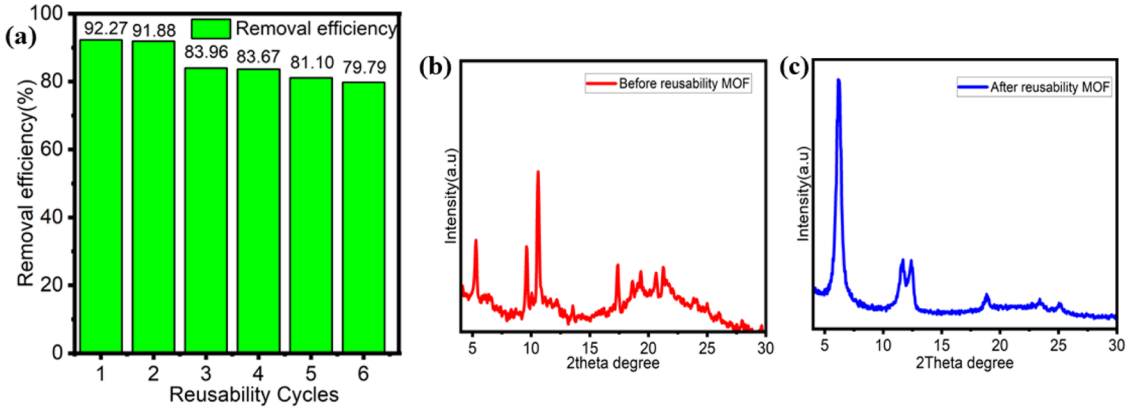

Figure 9. Reusability cycles of (a) 2D AlNiZn-LDH/BDC MOF and XRD pattern of 2D AlNiZn-LDH/BDC MOF (b) before and (c) after reusability.

https://doi.org/10.1021/acsomega.3c10524
ACS Omega 2024, 9, 16334−16345

4. CONCLUSIONS

In this study, we demonstrated an efficient and innovative approach for transforming *in situ* LDH into a MOF *via* a single-step hydrothermal method. The pristine 2D AlNiZn-LDH nanosheet, containing embedded metal ions and surficial hydroxyl groups (OH^-), displayed an excellent affinity with *p*-terephthalic acid, facilitating its successful conversion into a MOF as confirmed by the p-XRD technique. The resulting prepared MOF contains carboxylate (COO^-) and hydroxyl groups (OH^-), along with buried metal ion (M^{n+}) and aromatic ring species, which prove highly effective for the removal of cationic dyes from water. The composite has shown exceptional removal efficiency, achieving a rapid 92.27% removal of 10 ppm aqueous MB within 30 min, outperforming the pristine LDH. The equilibrium isotherm data best fits the Langmuir model, indicating a mechanism where MB adsorption occurs through a uniform distribution forming monolayers on the adsorbent surface. Moreover, the adsorbent indicated excellent reusability, retaining its effectiveness across six adsorption and desorption cycles. Comprehensive characterization techniques employed in this study have unequivocally validated the successful conversion of LDH into an MOF, highlighting its promising potential for the efficient adsorption of MB, a representative cationic dye, from contaminated water sources.

■ ASSOCIATED CONTENT

Supporting Information

The Supporting Information is available free of charge at https://pubs.acs.org/doi/10.1021/acsomega.3c10524.

UV−vis spectra of 2D AlNiZn-LDH for different factors: (a) pH, (b) contact time, (c) dye concentration, and (d) temperature (Figure S1); adsorption capacity of 2D AlNiZn-LDH and 2D AlNiZn-LDH/BDC MOF for different factors: (a) pH, (b) contact time, (c) dye concentration, and (d) temperature (Figure S2); effect of adsorbent (2D AlNiZn-LDH/BDC MOF) concentration on adsorption capacity (Figure S3); isothermal models for 2D AlNiZn-LDH and 2D AlNiZn-LDH/BDC MOF (Table S1); adsorption kinetic models (Table S2); thermodynamic parameters for 2D AlNiZn-LDH and 2D AlNiZn-LDH/BDC MOF (Table S3); ζ-Potential spectra of (a) 2D AlNiZn-LDH and (b) 2D AlNiZn-LDH/BDC MOF (Figure S4) (PDF)

■ AUTHOR INFORMATION

Corresponding Author

Manzar Sohail − *Department of Chemistry, National University of Sciences and Technology, Islamabad 44000, Pakistan;* orcid.org/0000-0003-1457-2491; Email: manzar.sohail@sns.nust.edu.pk

Authors

Ghulam Murtaza − *Department of Chemistry, National University of Sciences and Technology, Islamabad 44000, Pakistan*

Syed Shoaib Ahmad Shah − *Department of Chemistry, National University of Sciences and Technology, Islamabad 44000, Pakistan;* orcid.org/0000-0003-1741-6048

Asad Mumtaz − *Department of Chemistry, National University of Sciences and Technology, Islamabad 44000, Pakistan;* orcid.org/0000-0001-6517-8932

Ghayoor Abbas Chotana − *Department of Chemistry and Chemical Engineering, Syed Babar Ali School of Science and Engineering, Lahore University of Management Sciences, Lahore 54792, Pakistan;* orcid.org/0000-0003-2634-0698

Ayman Nafady − *Chemistry Department, College of Science, King Saud University, Riyadh 11451, Saudi Arabia*

Md A. Wahab − *Energy and Process Engineering Laboratory, School of Mechanical, Medical and Process Engineering, Faculty of Science, Queensland University of Technology (QUT), Brisbane, QLD 4000, Australia*

Complete contact information is available at: https://pubs.acs.org/10.1021/acsomega.3c10524

Author Contributions

G.M. performed the investigation and wrote the original draft. S.S.A.S. was responsible for the formal analysis and conceptualization. A.M. wrote and reviewed the manuscript and performed the kinetic studies. A.N. wrote and reviewed the manuscript and acquired funds. G.A. performed the formal analysis and reviewed and edited the manuscript. M.S. conceptualized the study, wrote, reviewed, and edited the manuscript, supervised the study, and performed funding acquisition. Md.A.W. was responsible for reviewing, writing, and editing the manuscript.

Notes

The authors declare no competing financial interest.

■ ACKNOWLEDGMENTS

The authors extend their sincere appreciation to Researchers Supporting Project number (RSP2024R79), King Saud University, Riyadh, Saudi Arabia.

■ REFERENCES

(1) Lu, H.; Zhang, L.; Wang, B.; Long, Y.; Zhang, M.; Ma, J.; Khan, A.; Chowdhury, S. P.; Zhou, X.; Ni, Y. Cellulose-supported magnetic Fe 3 O 4−MOF composites for enhanced dye removal application. *Cellulose* **2019**, *26*, 4909−4920.

(2) Briffa, J.; Sinagra, E.; Blundell, R. Heavy metal pollution in the environment and their toxicological effects on humans. *Heliyon* **2020**, *6* (9), No. e04691. Zafar, H. K.; Sohail, M.; Nafady, A.; Ostrikov, K. K.; Will, G.; Wahab, M. A.; O'Mullane, A. P. S-doped copper selenide thin films synthesized by chemical bath deposition for photoelectrochemical water splitting. *Appl. Surf. Sci.* **2023**, *641*, No. 158505.

(3) Shah, S. S. A.; Sohail, M.; Murtza, G.; Waseem, A.; Rehman, Au.; Hussain, I.; Bashir, M. S.; Alarfaji, S. S.; Hassan, A. M.; Nazir, M. A.; et al. Recent trends in wastewater treatment by using metal-organic frameworks (MOFs) and their composites: A critical view-point. *Chemosphere* **2024**, *349*, No. 140729.

(4) Shahzad, K.; Najam, T.; Bashir, M. S.; Nazir, M. A.; ur Rehman, A.; Bashir, M. A.; Shah, S. S. A. Fabrication of Periodic Mesoporous Organo Silicate (PMOS) composites of Ag and ZnO: Photo-catalytic degradation of methylene blue and methyl orange. *Inorg. Chem. Commun.* **2021**, *123*, No. 108357.

(5) Cheng, Z.; Liao, J.; He, B.; Zhang, F.; Zhang, F.; Huang, X.; Zhou, L. One-step fabrication of graphene oxide enhanced magnetic composite gel for highly efficient dye adsorption and catalysis. *ACS Sustainable Chem. Eng.* **2015**, *3* (7), 1677−1685.

(6) Zeng, H.; Zhang, W.; Deng, L.; Luo, J.; Zhou, S.; Liu, X.; Pei, Y.; Shi, Z.; Crittenden, J. Degradation of dyes by peroxymonosulfate activated by ternary CoFeNi-layered double hydroxide: Catalytic performance, mechanism and kinetic modeling. *J. Colloid Interface Sci.* **2018**, *515*, 92−100.

(7) Lazar, P.; Karlicky, F.; Jurecka, P.; Kocman, M.; Otyepková, E.; Šafářová, K.; Otyepka, M. Adsorption of small organic molecules on graphene. *J. Am. Chem. Soc.* **2013**, *135* (16), 6372−6377.
(8) Gao, L.; Gao, T.; Zhang, Y.; Hu, T. A bifunctional 3D porous Zn-MOF: Fluorescence recognition of Fe3+ and adsorption of congo red/methyl orange dyes in aqueous medium. *Dyes Pigm.* **2022**, *197*, No. 109945.
(9) Nazir, M. A.; Najam, T.; Jabeen, S.; Wattoo, M. A.; Bashir, M. S.; Shah, S. S. A.; ur Rehman, A. Facile synthesis of Tri-metallic layered double hydroxides (NiZnAl-LDHs): Adsorption of Rhodamine-B and methyl orange from water. *Inorg. Chem. Commun.* **2022**, *145*, No. 110008.
(10) Salem, M. A.; Khan, A. M.; Manea, Y. K.; Wani, A. A. Nano chromium embedded in f-CNT supported CoBi-LDH nanocomposites for selective adsorption of Pb2+ and hazardous organic dyes. *Chemosphere* **2022**, *289*, No. 133073.
(11) Wang, X.; Cheng, B.; Zhang, L.; Yu, J.; Li, Y. Synthesis of MgNiCo LDH hollow structure derived from ZIF-67 as superb adsorbent for Congo red. *J. Colloid Interface Sci.* **2022**, *612*, 598−607.
(12) Senguttuvan, S.; Janaki, V.; Senthilkumar, P.; Kamala-Kannan, S. Polypyrrole/zeolite composite−A nanoadsorbent for reactive dyes removal from synthetic solution. *Chemosphere* **2022**, *287*, No. 132164.
(13) Zhai, Q.-G.; Bu, X.; Zhao, X.; Li, D.-S.; Feng, P. Pore space partition in metal−organic frameworks. *Acc. Chem. Res.* **2017**, *50* (2), 407−417.
(14) Fan, W.; Wang, K.-Y.; Welton, C.; Feng, L.; Wang, X.; Liu, X.; Li, Y.; Kang, Z.; Zhou, H.-C.; Wang, R.; Sun, D. Aluminum metal−organic frameworks: From structures to applications. *Coord. Chem. Rev.* **2023**, *489*, No. 215175.
(15) Patra, S.; Mishra, S.; Parhi, B.; Mishra, H.; Swain, S. K. Role of transition metal nanocomposites in organic reactions: A state of art as an alternative to conventional catalysts. *Results Chem.* **2023**, *6*, No. 101172. Fiaz, M.; Sohail, M.; Nafady, A.; Will, G.; Wahab, M. A. A facile two-step hydrothermal preparation of 2D/2D heterostructure of Bi2WO6/WS2 for the efficient photodegradation of methylene blue under sunlight. *Environ. Res.* **2023**, *234*, No. 116550.
(16) Hu, H.; Wageh, S.; Al-Ghamdi, A. A.; Yang, S.; Tian, Z.; Cheng, B.; Ho, W. NiFe-LDH nanosheet/carbon fiber nanocomposite with enhanced anionic dye adsorption performance. *Appl. Surf. Sci.* **2020**, *511*, No. 145570.
(17) Yilmaz, G.; Yam, K. M.; Zhang, C.; Fan, H. J.; Ho, G. W. In Situ Transformation of MOFs into Layered Double Hydroxide Embedded Metal Sulfides for Improved Electrocatalytic and Supercapacitive Performance. *Adv. Mater.* **2017**, *29* (26), No. 1606814.
(18) Ming, Y.; Kumar, N.; Siegel, D. J. Water adsorption and insertion in MOF-5. *ACS Omega* **2017**, *2* (8), 4921−4928.
(19) Ahmad, K.; Nazir, M. A.; Qureshi, A. K.; Hussain, E.; Najam, T.; Javed, M. S.; Shah, S. S. A.; Tufail, M. K.; Hussain, S.; Khan, N. A.; et al. Engineering of Zirconium based metal-organic frameworks (Zr-MOFs) as efficient adsorbents. *Mater. Sci. Eng., B* **2020**, *262*, No. 114766.
(20) Zhang, K.; Yang, Z.; Mao, X.; Chen, X.-L.; Li, H.-H.; Wang, Y.-Y. Multifunctional textiles/metal− organic frameworks composites for efficient ultraviolet radiation blocking and noise reduction. *ACS Appl. Mater. Interfaces* **2020**, *12* (49), 55316−55323.
(21) Hussain, S.; Yang, X.; Aslam, M. K.; Shaheen, A.; Javed, M. S.; Aslam, N.; Aslam, B.; Liu, G.; Qiao, G. Robust TiN nanoparticles polysulfide anchor for Li−S storage and diffusion pathways using first principle calculations. *Chem. Eng. J.* **2020**, *391*, No. 123595.
(22) Ahmad, N.; Younus, H. A.; Chughtai, A. H.; Van Hecke, K.; Khattak, Z. A.; Gaoke, Z.; Danish, M.; Verpoort, F. Synthesis of 2D MOF having potential for efficient dye adsorption and catalytic applications. *Catal. Sci. Technol.* **2018**, *8* (16), 4010−4017.
(23) Shah, S. S. A.; Najam, T.; Cheng, D.; Hafeez, A.; Lu, Y.; Waseem, A. Nano-metal organic frame work an excellent tool for biomedical imaging. *Curr. Med. Imaging Rev.* **2018**, *14* (5), 669−674.
(24) Najam, T.; Shah, S. S. A.; Ding, W.; Deng, J.; Wei, Z. Enhancing by nano-engineering: Hierarchical architectures as oxygen reduction/evolution reactions for zinc-air batteries. *J. Power Sources* **2019**, *438*, No. 226919.
(25) Nazir, M. A.; Khan, N. A.; Cheng, C.; Shah, S. S. A.; Najam, T.; Arshad, M.; Sharif, A.; Akhtar, S.; ur Rehman, A. Surface induced growth of ZIF-67 at Co-layered double hydroxide: Removal of methylene blue and methyl orange from water. *Appl. Clay Sci.* **2020**, *190*, No. 105564.
(26) Nazir, M. A.; Khan, N. A.; Cheng, C.; Shah, S. S. A.; et al. Surface induced growth of ZIF-67 at Co-layered double hydroxide: Removal of methylene blue and methyl orange from water. *Appl. Clay Sci.* **2020**, *190*, No. 105564.
(27) Yan, A.-X.; Yao, S.; Li, Y.-G.; Zhang, Z.-M.; Lu, Y.; Chen, W.-L.; Wang, E.-B. Incorporating Polyoxometalates into a Porous MOF Greatly Improves Its Selective Adsorption of Cationic Dyes. *Chem. - Eur. J.* **2014**, *20* (23), 6927−6933.
(28) Starukh, G.; Rozovik, O.; Oranska, O. Organo/Zn-Al LDH nanocomposites for cationic dye removal from aqueous media. *Nanoscale Res. Lett.* **2016**, *11*, No. 228.
(29) Sharifi-Bonab, M.; Aber, S.; Salari, D.; Khodam, F. Synthesis of CoZnAl-layered double hydroxide/graphene oxide nanocomposite for the removal of methylene blue: Kinetic, thermodynamic, and isotherm studies. *Environ. Prog. Sustainable Energy* **2020**, *39* (2), No. e13316.
(30) Abd El-Monaem, E. M.; Hosny, M.; Eltaweil, A. S. Synergistic effect between adsorption and Fenton-like degradation on CoNiFe-LDH/ZIF-8 composite for efficient degradation of doxycycline. *Chem. Eng. Sci.* **2024**, *287*, No. 119707.
(31) Shi, Q.; Cheng, M.; Liu, Y.; Wang, J.; Zhang, G.; Li, L.; Du, L.; Wang, G.; Liu, H. In-situ generated MOFs with supportive LDH substrates and their derivatives for photo-electrocatalytic energy production and electrochemical devices: Insights into synthesis, function, performance and mechanism. *Coord. Chem. Rev.* **2024**, *499*, No. 215500.
(32) Zha, X.; Sun, W.; Liu, J.; Sun, G.; Lu, S.; Wang, Y. Three-dimensional hydrangea-like layered double hydroxide anchoring hollow metal organic-framework for efficient adsorption of 2, 4-dichlorophenoxyacetic acid. *Mater. Today Chem.* **2024**, *35*, No. 101883.
(33) Chakraborty, A.; Acharya, H. Selective Removal of Anionic Dyes by Metal−Organic Framework-Anchored CoAl-Layered Double Hydroxide Nanosheets. *ACS Appl. Nano Mater.* **2021**, *4* (11), 12561−12575.
(34) Hu, M.; Lou, H.; Yan, X.; Hu, X.; Feng, R.; Zhou, M. In-situ fabrication of ZIF-8 decorated layered double oxides for adsorption and photocatalytic degradation of methylene blue. *Microporous Mesoporous Mater.* **2018**, *271*, 68−72.
(35) Hines, D. R.; Solin, S.; Costantino, U.; Nocchetti, M. Physical properties of fixed-charge layer double hydroxides. *Phys. Rev. B* **2000**, *61* (17), No. 11348.
(36) Peng, L.; Wu, S.; Yang, X.; Hu, J.; Fu, X.; Huo, Q.; Guan, J. Application of metal organic frameworks M (bdc)(ted) 0.5 (M = Co, Zn, Ni, Cu) in the oxidation of benzyl alcohol. *RSC Adv.* **2016**, *6* (76), 72433−72438.
(37) Kong, L.; Yan, Q.; Wang, Y.; Wang, Q.; Andrews, C. B.; Zheng, C. Self-supported trimetallic NiZnLa nanosheets on hierarchical porous graphene oxide-polymer composite fibers for enhanced phosphate removal from water. *J. Colloid Interface Sci.* **2022**, *628*, 807−818.
(38) Wang, W.; Kang, Y.; Cui, C.; Lv, X.; Wang, Z.; Wang, B.; Tan, Y.; Jiao, S.; Pang, G. Fabrication of underliquid dual superlyophobic membrane via anchoring polyethersulfone nanoparticles on Zn-Ni-Co layered double hydroxide (LDH) nanowires with stainless steel mesh as supporter. *Sep. Purif. Technol.* **2022**, *294*, No. 121148.
(39) Cui, J.; Zhou, Z.; Xie, A.; Wang, Q.; Liu, S.; Lang, J.; Li, C.; Yan, Y.; Dai, J. Facile preparation of grass-like structured NiCo-LDH/PVDF composite membrane for efficient oil−water emulsion separation. *J. Membr. Sci.* **2019**, *573*, 226−233.
(40) Chen, Q.; Wang, X.; Wang, Z.; Cao, J.; Dai, J.; Wang, J.; Fatima-Ezzahra, E.; Huang, X. Partial Exchange between Inorganic and Organic Anions in MgAl Layered Double Hydroxide Nanosheets

https://doi.org/10.1021/acsomega.3c10524
ACS Omega 2024, 9, 16334−16345

for Humidity Sensing. *ACS Appl. Nano Mater.* **2022**, *5* (4), 4991−4997.
(41) Zhou, Y.; Chen, Y.; Liu, L.; Zhao, Q.; Jiang, T. Design and preparation of three-dimensional core-shell structures CF@ Cu-BDC@ NiCo-LDH for high-performance battery-type supercapacitors and oxygen evolution reaction. *J. Taiwan Inst. Chem. Eng.* **2023**, *144*, No. 104643.
(42) Nagendra, B.; Rosely, C. S.; Leuteritz, A.; Reuter, U.; Gowd, E. B. Polypropylene/layered double hydroxide nanocomposites: Influence of LDH intralayer metal constituents on the properties of polypropylene. *ACS Omega* **2017**, *2* (1), 20−31.
(43) Chakraborty, A.; Acharya, H. Facile synthesis of MgAl-layered double hydroxide supported metal organic framework nanocomposite for adsorptive removal of methyl orange dye. *Colloids Interface Sci. Commun.* **2018**, *24*, 35−39.
(44) Ahmadijokani, F.; Mohammadkhani, R.; Ahmadipouya, S.; Shokrgozar, A.; Rezakazemi, M.; Molavi, H.; Aminabhavi, T. M.; Arjmand, M. Superior chemical stability of UiO-66 metal-organic frameworks (MOFs) for selective dye adsorption. *Chem. Eng. J.* **2020**, *399*, No. 125346.
(45) Mahto, T. K.; Chandra, S.; Haldar, C.; Sahu, S. K. Kinetic and thermodynamic study of polyaniline functionalized magnetic mesoporous silica for magnetic field guided dye adsorption. *RSC Adv.* **2015**, *5* (59), 47909−47919.
(46) Lei, Y.; Zhang, J.; Liu, X.; Dai, Z.; Zhao, X. Gadolinium metal-organic frameworks realizing ultra-high adsorption capacity toward anionic dyes in aqueous solution. *J. Solid State Chem.* **2022**, *316*, No. 123563.
(47) Li, Y.; Yan, X.; Hu, X.; Feng, R.; Zhou, M. Trace pyrolyzed ZIF-67 loaded activated carbon pellets for enhanced adsorption and catalytic degradation of Rhodamine B in water. *Chem. Eng. J.* **2019**, *375*, No. 122003.
(48) Hu, H.; Liu, J.; Xu, Z.; Zhang, L.; Cheng, B.; Ho, W. Hierarchical porous Ni/Co-LDH hollow dodecahedron with excellent adsorption property for Congo red and Cr (VI) ions. *Appl. Surf. Sci.* **2019**, *478*, 981−990.
(49) Babapour, M.; Dehghani, M. H.; Alimohammadi, M.; Arjmand, M. M.; Salari, M.; Rasuli, L.; Mubarak, N. M.; Khan, N. A. Adsorption of Cr(VI) from aqueous solution using mesoporous metal-organic framework-5 functionalized with the amino acids: Characterization, optimization, linear and nonlinear kinetic models. *J. Mol. Liq.* **2022**, *345*, No. 117835.
(50) Wang, N.; Xu, X.; Li, H.; Yuan, L.; Yu, H. Enhanced selective adsorption of Pb (II) from aqueous solutions by one-pot synthesis of xanthate-modified chitosan sponge: behaviors and mechanisms. *Ind. Eng. Chem. Res.* **2016**, *55* (47), 12222−12231.
(51) Seera, S. D. K.; Kundu, D.; Gami, P.; Naik, P. K.; Banerjee, T. Synthesis and characterization of xylan-gelatin cross-linked reusable hydrogel for the adsorption of methylene blue. *Carbohydr. Polym.* **2021**, *256*, No. 117520.
(52) Chen, C.; Zhang, M.; Guan, Q.; Li, W. Kinetic and thermodynamic studies on the adsorption of xylenol orange onto MIL-101 (Cr). *Chem. Eng. J.* **2012**, *183*, 60−67.
(53) Liu, L.; Zhang, B.; Zhang, Y.; He, Y.; Huang, L.; Tan, S.; Cai, X. Simultaneous removal of cationic and anionic dyes from environmental water using montmorillonite-pillared graphene oxide. *J. Chem. Eng. Data* **2015**, *60* (5), 1270−1278.
(54) Soltani, R.; Marjani, A.; Shirazian, S. A hierarchical LDH/MOF nanocomposite: single, simultaneous and consecutive adsorption of a reactive dye and Cr (vi). *Dalton Trans.* **2020**, *49* (16), 5323−5335.
(55) Zhang, Y.-y.; Liu, Q.; Yang, C.; Wu, S.-c.; Cheng, J.-h. Magnetic aluminum-based metal organic framework as a novel magnetic adsorbent for the effective removal of minocycline from aqueous solutions. *Environ. Pollut.* **2019**, *255*, No. 113226.
(56) Alqadami, A. A.; Naushad, M.; Alothman, Z.; Ahamad, T. Adsorptive performance of MOF nanocomposite for methylene blue and malachite green dyes: kinetics, isotherm and mechanism. *J. Environ. Manage.* **2018**, *223*, 29−36.
(57) Kundu, D.; Mondal, S. K.; Banerjee, T. Development of β-cyclodextrin-cellulose/hemicellulose-based hydrogels for the removal of Cd (II) and Ni (II): synthesis, kinetics, and adsorption aspects. *J. Chem. Eng. Data* **2019**, *64* (6), 2601−2617.
(58) Zhu, D.; Liu, J.; Wang, L.; Du, Y.; Zheng, Y.; Davey, K.; Qiao, S.-Z. A 2D metal−organic framework/Ni (OH) 2 heterostructure for an enhanced oxygen evolution reaction. *Nanoscale* **2019**, *11* (8), 3599−3605.

https://doi.org/10.1021/acsomega.3c10524
ACS Omega 2024, 9, 16334−16345